JM RAPIDS

CrossMark

Destabilization of binary mixing layer in supercritical conditions

Nguyen Ly[1,†] and Matthias Ihme[1]

[1]Department of Mechanical Engineering, Stanford University, Stanford, CA 94305, USA

Compressible mixing layer instabilities are of importance to a wide range of environmental and industrial applications. Past studies have focused on either ideal-gas or real-fluid thermodynamic regimes of single-species mixing layers. However, mixing layers of binary mixtures at supercritical conditions, commonly encountered in fuel injection systems, introduce additional complexities due to the added compositional degree-of-freedom. Moreover, the effect of strong variations in thermodynamic response functions across the Widom line on the binary mixing layer stability remains poorly understood. Thus, the objective of this study is to examine the coupling between the hydrodynamic instability and the real-fluid thermodynamics across the Widom line and its effects on the overall binary mixing layer dynamics. To this end, we develop a linear stability analysis of the full binary-species compressible transport equations coupled with the PC-SAFT equation of state. Analysis shows the existence of a novel instability mechanism that arises from juxtapositioning of the Widom-line transition and the hydrodynamic inflection point. This novel thermodynamically induced instability mechanism has the net effect of destabilizing the binary mixing layer at lowering supercritical conditions towards the critical pressure point. This is in contrast to previous stability analyses of supercritical single-species mixing layers, where increasing pressure destabilizes the flow due to its effect on reducing the density stratification. The discovered thermodynamically induced instability mechanism of binary mixing flows highlights the need for an extension of classical instability criteria to incorporate the effect of strong variations in the thermodynamic response functions across the Widom line on mixing layer instability.

Key words: shear-flow instability

1. Introduction

The stability of parallel shear flows is well established in the fluid-mechanics community. The problem manifests both in the theoretical study of Kelvin–Helmholtz instabilities
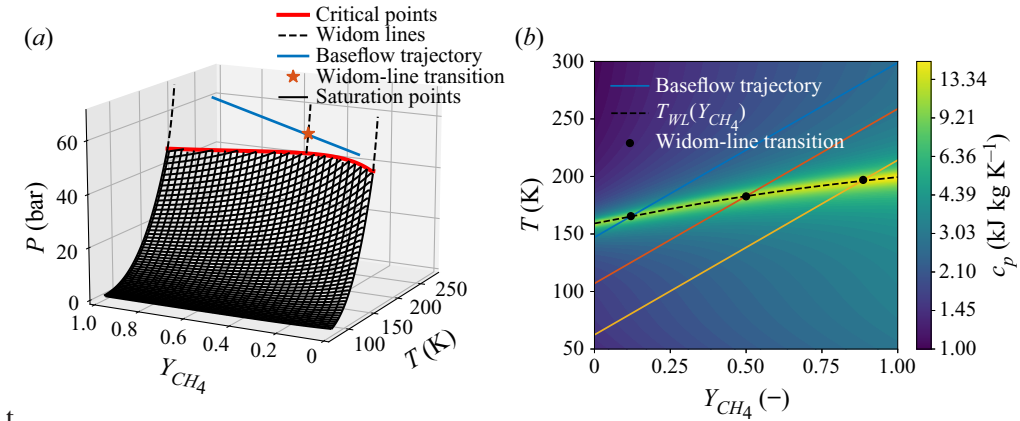
† Email address for correspondence: nguyenly@stanford.edu

Figure 1. (*a*) Thermodynamic regime diagram of CH_4/O_2 mixture at subcritical and supercritical conditions. Also plotted is the locus of thermodynamic conditions found in a representative isobaric baseflow. (*b*) Isobaric state space: isobaric projection of the supercritical thermodynamic regime diagram of CH_4/O_2 at $P = 60$ bar, showing contour of isobaric heat capacity (c_p). Also shown is the Widom-line transition temperature as a function of composition $T_{WL}(Y_{CH_4})$ and example isobaric thermodynamic trajectories of the baseflow.

and in environmental and engineering flows. Blumen (1970) studied the stability dynamics of a compressible shear flow with constant thermodynamic properties. In this regime, he showed that Fjørtoft's extension of Rayleigh's criterion, originally developed for incompressible shear layers, extends to the compressible flow regime. However, many engineering mixing flows involve binary and multispecies mixtures at trans- and supercritical conditions and thus feature complex thermodynamic response functions. The consideration of these effects is not covered by classical stability theory.

With increasing interest in high-pressure flow systems, much effort has been expended towards studying mixing flows at supercritical thermodynamic conditions. At these conditions, the fluids exhibit behaviours not found in subcritical conditions such as a sharp decrease in surface tension, resulting in diffused phase transition (Oschwald *et al.* 2006). At the thermodynamic critical point, the saturation line, which delineates liquid and vapour regions at subcritical conditions, extends to the Widom line in the supercritical regime. It represents a degenerate form of phase transition between supercritical gas-like and supercritical liquid-like phases (Simeoni *et al.* 2010), see figure 1(*a*). Therefore, across the Widom line, transition from a liquid-like to a gas-like regime occurs, giving rise to large gradients in thermodynamic and transport properties. These enhanced variations in the thermodynamic response functions have been found to promote instabilities in Rayleigh–Bénard convection, swirling jet flows, channel flows and boundary layers (Accary *et al.* 2005; Ly, Rusak & Wang 2018; Ren, Fu & Pecnik 2019*a*; Ren, Marxen & Pecnik 2019*b*). At increasing pressures, the distinction between supercritical gas-like and liquid-like phases diminishes, thus reducing the density variation across and lowering peak heat capacity at the Widom-line transition. In this regime, Zong *et al.* (2004) performed experimental investigations and conducted linear stability analysis (LSA) of supercritical single-species mixing flows of N_2. They concluded that at supercritical pressures, the dampening effect of the liquid–vapour interface is reduced and thus the single-species mixing layer becomes more unstable. Similarly, Roy & Segal (2010) performed experiments of N_2 injection at various sub/supercritical conditions and concluded that at supercritical conditions, the flow's density gradient reduced and that this behaviour strongly affects the length of the potential core.

Overall, in single-species mixing flow conditions, the destabilizing effect of increasing supercritical pressure has been attributed to its influence on the single-species mixing flow's hydrodynamics via the reduction in density stratification across the inflection point. However, the impact of the thermodynamic response functions, which are strong functions of pressure supercritical conditions, on binary and multispecies mixing flows has not been investigated in isolation. Considerations of strong variations in the thermodynamic response functions are of direct importance in binary mixing flows, where the density stratification is largely a function of the compositional difference across the inflection point and thus becomes more insensitive to increases in pressure. Furthermore, binary mixing layers introduce additional parametric complexities arising from the alignment of temperature and composition profiles across the binary mixing layer. These conditions determine the location of the Widom-line transition in the baseflow, see figure 1(*b*).

In this paper, we investigate the effect of the thermodynamic response functions on the stability of binary mixing layers at supercritical thermodynamic conditions. Specifically, we develop a LSA of the full multispecies compressible transport equations coupled with the PC-SAFT equation of state (EOS) (Gross & Sadowski 2001) to examine the interference of the strong variations in the thermodynamic response functions across the Widom line with the underlying binary mixing layer dynamics. To this end, baseflow conditions are selected to traverse the Widom line within the binary mixing layer, thus featuring degenerate phase transition and non-ideal thermodynamic and transport properties at the transition condition. Furthermore, by considering a binary mixing flow configuration of CH_4 and O_2, we maintain a similar level of momentum and density stratification across the binary mixing layer even at high supercritical pressures, where the differences between liquid-like densities and gas-like densities of each species are diminished. This allows us to isolate and to examine the effects of supercritical real-fluid thermodynamics across the Widom line on classical mixing layer instability, which are not investigated by past studies. Through this analysis, the enhanced sensitivity of the thermodynamic response functions across the Widom line is shown to stimulate secondary instability mechanisms that couple with the underlying hydrodynamic Kelvin–Helmholtz instability.

2. Mathematical formulation

2.1. *Governing equations*

To describe the supercritical binary mixing flow, we consider the non-dimensional form of the multispecies conservation equations for mass, species, momentum and energy in two dimensions for a binary mixture:

$$D_t \rho = -\rho \nabla \cdot \boldsymbol{u}, \tag{2.1a}$$

$$\rho D_t Y_F = \frac{1}{Pe} \nabla \cdot (\rho \alpha_m \nabla Y_F), \quad Y_O = 1 - Y_F, \tag{2.1b}$$

$$\rho D_t \boldsymbol{u} = -\frac{1}{Ma^2} \nabla P + \frac{1}{Re} \nabla \cdot \boldsymbol{\tau}, \quad \boldsymbol{\tau} = 2\mu \left(\boldsymbol{S} - \frac{1}{3}(\nabla \cdot \boldsymbol{u})\boldsymbol{I} \right), \tag{2.1c}$$

$$\rho D_t h_t = \frac{\gamma - 1}{\gamma} \partial_t P + \frac{Ec}{Re} \nabla \cdot (\boldsymbol{u} \cdot \boldsymbol{\tau}) + \nabla \cdot \left(\frac{\lambda}{PrRe} \nabla T + \frac{1}{Pe} \sum_{k=\{F,O\}} (\rho \alpha_m \nabla Y_k h_k) \right), \tag{2.1d}$$

where $D_t \equiv \partial_t + \boldsymbol{u} \cdot \nabla$ denotes the substantial derivative; $k = \{F, O\}$ is the species index of methane and oxygen, respectively; ρ is the density; T is the temperature; and

P is the pressure of the mixture. Here $h_t = h + Ec\|\boldsymbol{u}\|^2/2$ is the total specific enthalpy, where h is the mixture thermodynamic enthalpy; h_k is the partial enthalpy; $\boldsymbol{u} = (u, v)^{\mathrm{T}}$ is the velocity vector; Y_k is the mass fraction of species k; μ is the dynamic viscosity; λ is thermal conductivity; and α_m is the mixture-averaged diffusion coefficient. Here $\boldsymbol{S} = (\nabla\boldsymbol{u} + (\nabla\boldsymbol{u})^{\mathrm{T}})/2$ is the strain rate tensor.

Reference values for non-dimensionalization are selected as follows: spatial dimensions are scaled by the binary mixing layer's thickness $\tilde{\delta}$; $\tilde{u}_{ref}$ is the fluid velocity at the centreline of the baseflow, $\tilde{\rho}_{ref}, \tilde{\mu}_{ref}, \tilde{\lambda}_{ref}, \tilde{\alpha}_{ref}$ are the flow density, viscosity, conductivity, and mixture-averaged diffusion coefficient at the centreline of the baseflow, respectively; $\tilde{P}_{ref}$ is the pressure condition of the isobaric binary mixing flow; $\tilde{T}_{ref}$ is calculated as $\tilde{P}_{ref}/(\tilde{R}_{ref}\tilde{\rho}_{ref})$, where $\tilde{R}_{ref}$ is the gas constant computed from the composition at the centreline of the baseflow; $\tilde{h}_{ref}$ is calculated as $\tilde{c}_{p,ref}\tilde{T}_{ref}$, where $\tilde{c}_{p,ref}$ is the isobaric specific heat capacity calculated from centreline conditions of the baseflow. The reference isentropic expansion factor is $\gamma = \tilde{c}_{p,ref}/(\tilde{c}_{p,ref} - \tilde{R}_{ref})$. The Mach number (*Ma*), Reynolds number (*Re*), Prandtl number (*Pr*), Eckert number (*Ec*), Péclet number (*Pe*) are defined as

$$Ma = \frac{\tilde{u}_{ref}}{\sqrt{\tilde{P}_{ref}/\tilde{\rho}_{ref}}}, \quad Re = \frac{\tilde{\rho}_{ref}\tilde{u}_{ref}\tilde{\delta}}{\tilde{\mu}_{ref}}, \quad Pr = \frac{\tilde{\mu}_{ref}\tilde{c}_{p,ref}}{\tilde{\lambda}_{ref}}, \quad Ec = \frac{\tilde{u}_{ref}^2}{\tilde{c}_{p,ref}\tilde{T}_{ref}}, \quad Pe = \frac{\tilde{u}_{ref}\tilde{\delta}}{\tilde{D}_{ref}}.$$

$$(2.2a\text{--}e)$$

The method of Chung, Lee & Starling (1984) is used to calculated mixture viscosity and conductivity at elevated pressures, and the Chapman–Enskog theory (Kee, Coltrin & Glarborg 2005), along with the high-pressure correction of Takahashi (1975) is used to calculate the binary diffusivity. The thermodynamic variables ρ, T, P, h, h_k, along with species composition Y_F, are closed using the PC-SAFT EOS (Gross & Sadowski 2001). This state equation has been selected for its enhanced accuracy in predicting thermodynamic properties of dense fluids, such as the high-pressure supercritical conditions considered in the present work.

2.2. *Linear stability analysis*

Linear stability analysis of the full set of multispecies, compressible governing equations (2.1) is performed. For this, we use $\boldsymbol{Q} = [u, v, \rho, T, Y_F]^{\mathrm{T}}$ as the fundamental variables. All other secondary variables in the set of governing equations ($\boldsymbol{\Psi}(\boldsymbol{Q}) = [P, h, h_k, \mu, \lambda, \alpha_m]^{\mathrm{T}}$) are evaluated by either the PC-SAFT EOS or the kinetic models for transport properties.

Analysis of a constant-property binary mixing layer yields the scaling of the non-dimensional vertical growth rate $v = (xRe)^{-1/2}/2$, where x is the axial distance from the end of the splitter plate. Thus, at high Reynolds number, the vertical growth rate of the binary mixing layer is negligible compared with the axial velocity and the quasi-parallel assumption can be invoked (Michalke 1972).

We first linearize the governing equations by using a first-order expansion around a baseflow that is steady and fully developed in the streamwise direction, $\boldsymbol{Q}(\boldsymbol{x}, t) = \boldsymbol{Q_0}(y) + \epsilon\boldsymbol{Q_1}(\boldsymbol{x}, t)$, where $\boldsymbol{x} \equiv [x, y]^{\mathrm{T}}$. The derived thermodynamic and transport properties are

expanded as Taylor series truncated to first order, e.g.

$$\boldsymbol{\Psi}(\boldsymbol{Q}) \approx \boldsymbol{\Psi}(\boldsymbol{Q_0}) + \epsilon \left. \frac{\partial \boldsymbol{\Psi}}{\partial \boldsymbol{Q}} \right|_0 \boldsymbol{Q_1}. \tag{2.3}$$

When the divergence of the diffusive fluxes in the governing equations are considered, higher-order derivatives of the secondary properties are also needed. These derivatives are computed analytically from the PC-SAFT EOS and kinetic models using automatic differentiation (Maclaurin, Duvenaud & Adams 2015).

From the linearized equations, we introduce the normal mode assumption for perturbation waves with profiles in the y-direction, travelling and growing in x and t, respectively, $\boldsymbol{Q_1}(\boldsymbol{x}, t) = \hat{\boldsymbol{Q}}(y) \exp\{i(\alpha x - \omega t)\}$, where $\hat{\boldsymbol{Q}}$ is the vector of the perturbation wave profiles, and α and ω are the complex wavenumber and frequency, respectively. At this point, the linearized governing equations along with the boundary conditions, $\boldsymbol{Q_1}(x, y \to \pm\infty, t) = \boldsymbol{0}$, constitute an eigenvalue problem where the frequencies ω can be solved for each value of wavenumber α and *vice versa*. The eigenvalue problem is discretized using Chebyshev expansion (Schmid & Henningson 2001):

$$\hat{\boldsymbol{Q}}(y) = \sum_{n=1}^{N} \hat{\mathcal{Q}}_n \cos(n \cos^{-1}(\xi)), \quad y = \frac{\xi}{\sqrt{1 - \xi^2}}, \tag{2.4a,b}$$

where the coordinate transformation $y \to \xi$ is performed to map the infinite domain in $y \in (-\infty, \infty)$ to a finite domain in $\xi \in (-1, 1)$. Here $\hat{\mathcal{Q}}_n$ is the vector of the coefficients of the nth Chebyshev mode of the fundamental variables. With this, the problem is recast into a generalized linear eigenvalue problem, $\boldsymbol{A}(\alpha)\hat{\mathcal{Q}} = \omega \boldsymbol{B}(\alpha)\hat{\mathcal{Q}}$, which is solved using a LAPACK routine.

3. Results

3.1. *Baseflow construction*

In this study, binary mixing layers of O_2 and CH_4 are considered. The baseflow is constructed for different isobaric conditions by assuming hyperbolic tangent profiles for velocity, temperature and fuel mass fraction across the binary mixing layer:

$$u_0(y) = 1 + \Delta_u \tanh(y), \quad T_0(y) = T_{ctr} + \Delta_T \tanh(y), \quad Y_{F,0}(y) = 0.5(1 + \tanh(y)). \tag{3.1a–c}$$

Here, $\tilde{T}_{ctr}$ is the non-dimensional centreline temperature, which differs from unity due to real-fluid thermodynamics; Δ_T and Δ_u are the non-dimensional temperature and velocity difference across the binary mixing layer, respectively. The binary mixing layer thickness and differences in velocity and temperature are chosen to be representative of LOX/GCH$_4$ rocket injection conditions (Lux & Haidn 2009): $\tilde{\delta} = 1$ mm, $\tilde{u}_{ref} = 50$ m s^{-1}, $\Delta_u = 1.5$ and $\tilde{\Delta}_T \tilde{T}_{ref} = 0.8 \tilde{T}_{c,CH_4} = 152$ K, where $\tilde{T}_{c,CH_4} = 190$ K is the critical temperature of CH$_4$. To control the location of the Widom-line transition within the binary mixing layer, we modulate the centreline temperature T_{ctr}, in effect shifting the isobaric thermodynamic trajectory of the baseflow, whose intersection with the surface of the Widom lines is the degenerate phase transition condition that manifests in the baseflow (see figure 1). For the configurations studied in this paper, the typical Reynolds number is $Re \approx 6 \times 10^5$, which validates the use of the quasi-parallel assumption for $x \sim O(1)$.
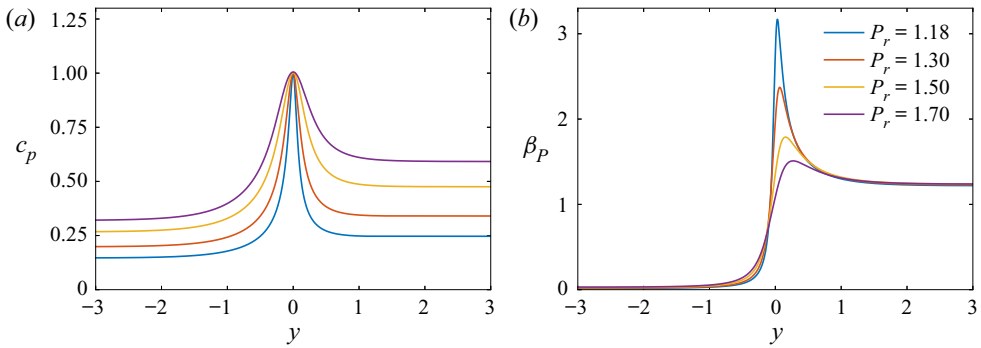
Figure 2. Baseflow profiles of (*a*) isobaric heat capacity and (*b*) isothermal compressibility as a function of pressure.

3.2. *Stability of real-fluid binary mixing flow*

To investigate the effects of supercritical real-fluid thermodynamics on the stability of the binary mixing layer, we perform LSA on isobaric baseflows with increasing pressure conditions from near the critical point, where effects of transitioning across the Widom line is strongest, to higher pressure levels, where these real-fluid effects are diminished. The pressure conditions studied are $P_r \equiv \tilde{P}_{ref}/\tilde{P}_{c,O_2} = \{1.18, 1.3, 1.5, 1.7, 2.0\}$. Here, the temperature profiles of the individual baseflows are designed such that transition across the Widom line occurs at the hydrodynamic inflection point (the centreline). Figure 2 plots the non-dimensional isobaric heat capacity, c_p, and isothermal compressibility, $\beta_P \equiv (\partial\rho/\partial P)_T/\rho$, at these supercritical pressure conditions. The strong variations in thermodynamic response functions across the degenerate phase transition condition at the centreline is signified by the peaks in heat capacity and compressibility. With increasing pressure, the distinction between supercritical liquid-like and gas-like states diminishes and these peaks become less pronounced.

With increasing pressure, we found a competition between a backward- and a forward-travelling eigenmode, whose profiles are plotted in figure 3(*a*). In both eigenmodes, the structure of the Kelvin–Helmholtz instability is present as a smooth peak in perturbation magnitude. However, the backward-travelling eigenmodes (characterized by below-unity phase speed) also feature a sharp peak of perturbation magnitude localized at the centreline, where the transition across the Widom line occurs and thus the sensitivities of the thermodynamic response functions are greatly enhanced (as highlighted in figure 2). In contrast, this thermodynamically induced instability is not present in the forward-travelling eigenmodes (characterized by above-unity phase speed). Instead, the effects of thermodynamics across the Widom line manifest as an attenuation of the perturbation magnitude at the centreline (the location of Widom-line crossing) due to the damping effect of the increased heat capacity. Thus, we hypothesize that these two competing eigenmodes represent two different arrangements between the near-critical real-fluid state and the classical binary mixing layer instability: the former is dominant for the backward-travelling eigenmode, while the latter is dominant for the forward-travelling eigenmode. Note that within each of the eigenmodes, the relative dominance of thermodynamically induced instability and hydrodynamically induced instability is also a function of wavenumber α, where the former is more significant at high wavenumbers and the latter at low wavenumbers. To evaluate the interaction between the thermodynamically induced and the hydrodynamically induced instability mechanisms,
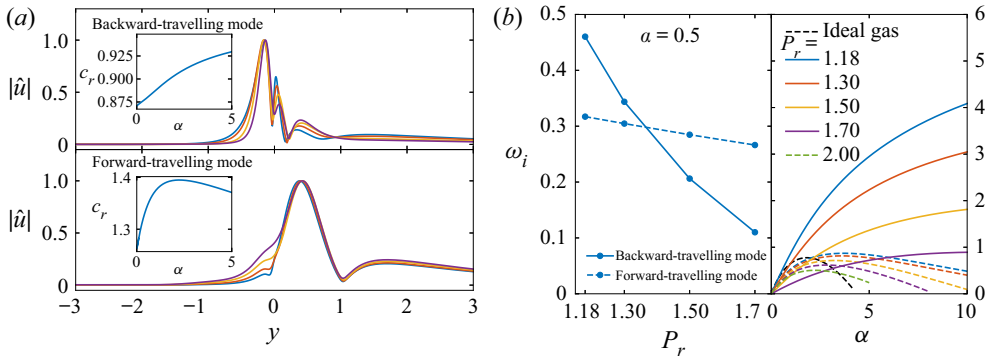
Figure 3. (*a*) Profiles of axial velocity perturbation mode for the two dominant eigenmodes for $P_r = 1.18 - 1.70$, $\alpha = 0.5$. Insets show the phase speed $c_r \equiv \omega_r/\alpha$ as a function of wavenumber for these two eigenmodes. (*b*) Temporal growth rate: competition between growth rates of the two dominant eigenmodes as a function of pressure and wavenumber.

in figure 3(*a*), the choice of $\alpha = 0.5$ is made so that both instability mechanisms have comparable influence on the eigenmodes.

As the pressure increases beyond the critical value and the enhanced sensitivities of the thermodynamic response functions across the Widom line are suppressed, the temporal growth rate at $\alpha = 0.5$ of the backward-travelling, thermodynamic-dominant eigenmode is reduced and eventually, at $P_r \approx 1.37$, is overtaken by the forward-travelling, hydrodynamic-dominant eigenmode, see the left panel of figure 3(*b*). At sufficiently high supercritical condition, $P_r \approx 2.00$, the effect of enhanced thermodynamic sensitivity across the Widom line is diminished, resulting in the vanishing of the backward-travelling eigenmode, which is dominated by the thermodynamically induced instability mechanism. Furthermore, this competition between the backward-travelling and forward-travelling eigenmodes is also influenced by the wavenumber, as evident by the distinction between their dispersion relations shown in the right panel of figure 3(*b*). Specifically, the growth rate of the forward-travelling eigenmode decays faster compared with that of the backward-travelling eigenmode at high wavenumbers, resulting in a wider band of unstable wavenumbers for the backward-travelling eigenmode.

We found that the net effect of increasing pressure beyond the critical point is to stabilize the binary mixing layer, as presented by the uniform reduction of the maximum temporal growth rate at all wavenumbers at high pressure in figure 3(*b*). This behaviour is uncovered thanks to the focus on binary mixing layers and is in contrast with past stability analyses of supercritical single-species mixing layer, where at increasing pressure conditions, the flow was found to destabilize due to a reduction in the density stratification across the single-species mixing layer (Zong *et al.* 2004). Furthermore, we note that the emergence of a dual-mode instability has also been observed by Ren *et al.* (2019*b*) in supercritical compressible single-species boundary-layer flows. Specifically, they discovered that in addition to the Tollmien–Schlichting instability mode (Mode I), an inviscid mode (Mode II) emerges for the baseflows that cross the Widom line. Similar to the thermodynamically dominated backward-travelling eigenmode in the present analysis, Mode II features much higher growth rates and a wider band of unstable frequencies. Thus, they showed that the introduction of dual-mode instability by Widom-line dynamics has a net effect of destabilizing the boundary-layer flow. This is in agreement with the present results of mixing layer instability.
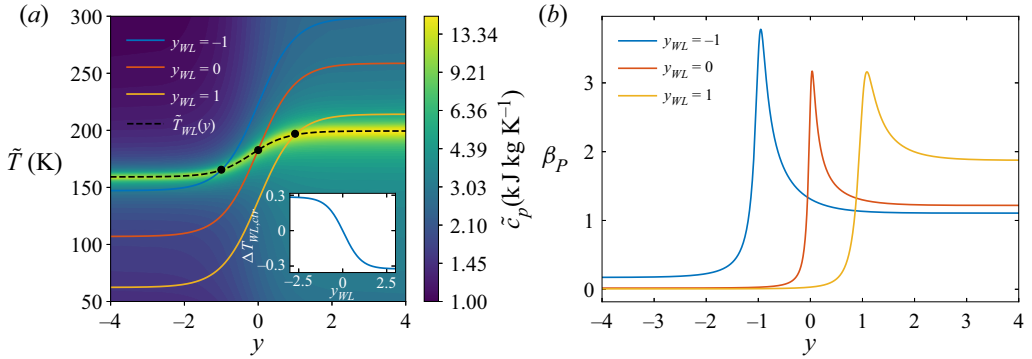
945 R2-7

Figure 4. (*a*) For a given pressure condition ($P_r = 1.18$), alignment between baseflow's temperature profile ($\tilde{T}_0(y)$, coloured lines) and the profile of local Widom-line transition temperatures ($\tilde{T}_{WL}(Y_{F,0}(y))$, black line) gives rise to local manifestation of degenerate phase transition conditions at various prescribed locations y_{WL} (black markers). Three examples of baseflows are given for $y_{WL} = \{-1, 0, 1\}$. Inset shows the relative attunement of the centreline temperature with the Widom-line transition temperature, $\Delta T_{WL,ctr} \equiv (\tilde{T}_0(0) - \tilde{T}_{WL}(0))/\tilde{T}_{WL}(0)$, for baseflows with different prescribed y_{WL}. (*b*) Profiles of isothermal compressibility for three example baseflows with various prescribed locations of Widom-line transition, demonstrating the enhanced sensitivity of the thermodynamic response.

3.3. *Attunement of Widom-line transition with binary mixing layer instability*

To investigate the role of Widom-line dynamics on destabilizing the flow through the thermodynamically induced instability mechanism, we perform LSA for near-critical ($P_r = 1.18$) baseflow that exhibits a degenerate phase transition at various prescribed locations y_{WL}, such that $\tilde{T}_0(y_{WL}) = \tilde{T}_{WL}(Y_{F,0}(y_{WL}))$. Specifically, figure 4(*a*) illustrates how the alignment between the location of Widom-line transition temperature, which is a function of local composition $\tilde{T}_{WL}(Y_{F,0}(y))$, with the temperature profile of the baseflow determines the location where degenerate phase transition occurs. Thus, through a shift in the baseflow's temperature profile by varying $\tilde{T}_{ctr}$ and keeping $\tilde{\Delta}_T$ constant, the location of degenerate phase transition y_{WL} is controlled. The relationship between $\tilde{T}_{ctr}$ and y_{WL} is shown in the inset of figure 4(*a*). Here, we note that shifting y_{WL} away from zero results in a detuning of the local thermodynamic condition at the inflection point of the baseflow away from the Widom-line transition condition. This allows us to evaluate the coupling between thermodynamic response (shown in figure 4*b*) with the underlying binary mixing layer instability, which manifests around the baseflow's inflection point at the centreline. Furthermore, note that due to the tanh-profiles of the baseflow's temperature and CH_4 mass fraction, as y_{WL} shifts deep into one of the two streams, the entirety of either stream will be at the Widom-line transition condition. Therefore, increasing or decreasing y_{WL} past ± 3 has negligible effect on the baseflow and thus on its stability characteristics.

Figure 5 plots the most unstable eigenmode for the axial velocity perturbation $|\hat{u}|$ and the reconstructed perturbation field at $\alpha = 0.5$ and $P_r = 1.18$, for $y_{WL} = 0, -0.5, -1.0, -3.0$. Here, the eigenmodes are normalized by their maximum amplitude and the eigenmode for the ideal-gas configuration is also plotted for reference. Note that comparisons between the magnitudes of the eigenmodes in figure 5 should not be performed because eigenmodes have no absolute scale in the LSA framework. Through these visualizations, we note the superposition of two different instability mechanisms near the centreline. One is the classical binary mixing layer instability that arises from the
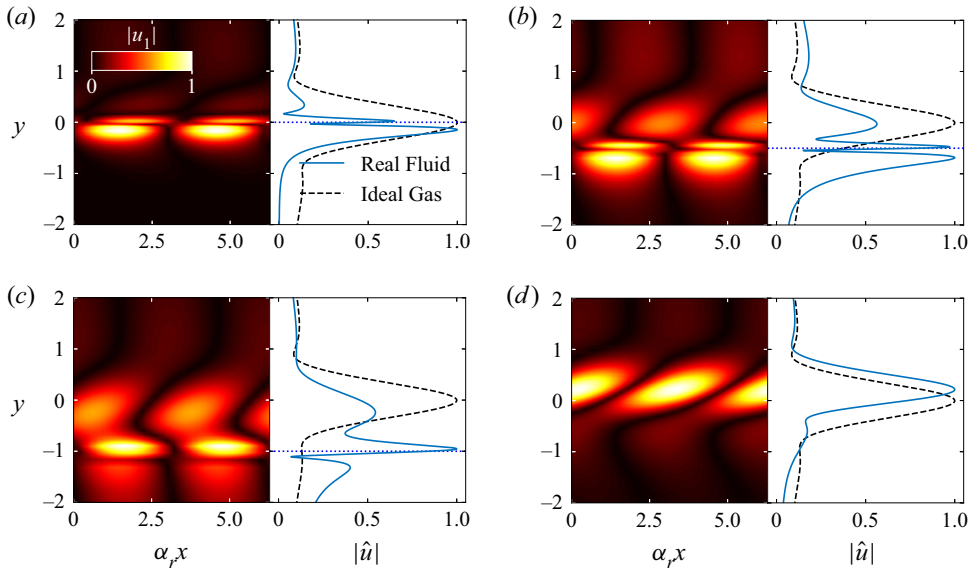
Figure 5. Reconstructed axial velocity perturbation u_1 (left side of graphs) and corresponding profiles of axial velocity perturbation mode $| \hat{u} |$ (right side of graphs) at $\alpha = 0.5$ for cases with $P_r = 1.18$ and $y_{WL} = \{0, -0.5, -1.0, -3.0\}$. (a) $y_{WL} = 0$. (b) $y_{WL} = -0.5$. (c) $y_{WL} = -1.0$. (d) $y_{WL} = -3.0$.

baseflow's inflection point, corresponding to the upper and smoother structure. The other is the thermodynamically induced instability that arises from the sharp variations in thermodynamic response functions, corresponding to the lower and sharper structure. As the Widom-line transition location y_{WL} shifts away from the centreline, the classical binary mixing layer instability remains at the inflection point at $y = 0$. In contrast, the location of the thermodynamically induced instability shifts in accordance with y_{WL}, see the evolution of the reconstructed axial velocity perturbation as y_{WL} is varied in the four panels of figure 5. Concurrently, with detuning of the Widom-line transition location y_{WL} away from the centreline, the classical binary mixing layer instability is amplified compared with the thermodynamically induced instability. This is caused by the thermal shielding effect of enhanced heat capacity across the Widom-line transition being lessened at the centreline. In contrast, as y_{WL} shifts away from the centreline, the thermodynamically induced instability is attenuated compared with the hydrodynamically induced instability, as there is a reduction in thermodynamic-property gradient required to activate the regions of high sensitivity in the thermodynamic response functions. Eventually, when $y_{WL} = -3$, the thermodynamically induced instability vanishes and the perturbation mode recovers towards that of the ideal-gas Kelvin–Helmholtz instability.

Overall, the net effect of aligning the Widom-line transition condition with the binary mixing layer's hydrodynamic inflection point is to destabilize the flow by introduction of the thermodynamically induced instability mechanism, see figure 6. Specifically, as y_{WL} shifts away from zero, variations in the thermodynamic response functions become less prominent at the hydrodynamic inflection point at the centreline. This effect leads to the reduction and eventual vanishing of the thermodynamic-dominant backward-travelling eigenmode as well as the tightening of the instability envelope of the hydrodynamic-dominant forward-travelling eigenmode. Eventually, when y_{WL} is
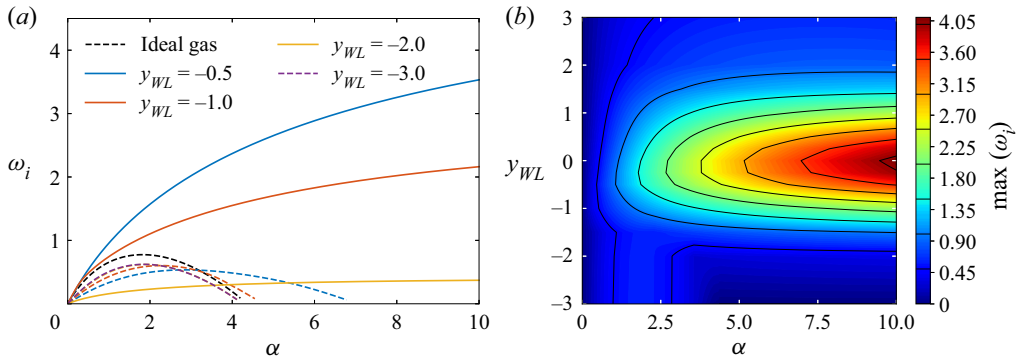
Figure 6. (*a*) Destabilizing influence of the alignment between thermodynamic Widom-line transition point and the binary mixing layer hydrodynamics on the temporal growth rate. Solid lines indicate backward-travelling eigenmode and dashedlines forward-travelling eigenmode. (*b*) Maximum temporal growth rate as a function of wavenumber α and location of Widom-line transition y_{WL}. Results are shown for $P_r = 1.18$.

sufficiently far away from the inflection point, the effects of the thermodynamic response functions on the binary mixing layer hydrodynamics vanishes and the instability envelope recovers towards that of the ideal-gas binary mixing layer instability.

4. Conclusions

The stability dynamics of binary mixing layers at supercritical pressure conditions was studied using LSA, in which real-fluid effects were considered using the PC-SAFT EOS. Specific focus was placed on examining the effects of strong variations in thermodynamic response functions across the Widom-line transition on the underlying binary mixing flow instability.

Results from the stability analysis show behaviours substantially different from previous studies of single-species mixing flows at supercritical conditions and of classical compressible mixing flows in ideal-gas conditions. Specifically, when the Widom-line transition location is colocated with the binary mixing layer's inflection point, we showed that the binary mixing layer is destabilized by the effects of supercritical real-fluid thermodynamics at the degenerate phase transition condition. Furthermore, it is shown that the destabilizing effect of supercritical real-fluid thermodynamics on binary mixing flows is brought about as a result of strong variations in the thermodynamic response functions at the Widom-line transition, which, when in close proximity with the binary mixing layer's inflection point, can take advantage of the existing flow perturbations to develop into a new instability mechanism that interacts with the existing Kelvin–Helmholtz instability. Thus, the strength of this thermodynamically induced instability is directly correlated to (*a*) the strength of real-fluid thermodynamic effects across the Widom-line transition, which diminishes with increasing pressure past the critical point and (*b*) the attunement between the location of Widom-line transition with the inflection point of the underlying binary mixing layer.

The coexistence of the thermodynamically induced and the hydrodynamically induced instability mechanisms uncovered in the present paper for supercritical mixing flows bears striking analogies with the dual-mode instability behaviour of supercritical boundary layers observed by Ren *et al.* (2019*b*). Thus, the results of the present study highlight the need for fundamental research into the universal coupling between Widom-line dynamics and hydrodynamic instabilities, as well as for an extension of classical instability criteria

(e.g. Rayleigh criterion and Fjørtoft's extension) to incorporate the effect of real-fluid thermodynamic response functions.

Finally, the exploitation of this instability mechanism offers opportunities for improving fuel injection systems operating at high pressures, such as diesel and rocket engines (Mayer *et al.* 2003; Koukouvinis *et al.* 2020). Specifically, while Banuti & Hannemann (2016) demonstrated that the mixing performance in single-fluids injectors can be improved by the potential core crossing the Widom line axially, we show in this paper that binary mixing flows feature another mechanism for enhanced mixing by crossing the Widom line vertically across the splitter plate.

Declaration of interests. The authors report no conflict of interest.

Author ORCIDs.

Nguyen Ly https://orcid.org/0000-0002-9032-6404;

Matthias Ihme https://orcid.org/0000-0002-4158-7050.

REFERENCES

ACCARY, G., RASPO, I., BONTOUX, P. & ZAPPOLI, B. 2005 Stability of a supercritical fluid diffusing layer with mixed boundary conditions. *Phys. Fluids* **17** (10), 104105.

BANUTI, D.T. & HANNEMANN, K. 2016 The absence of a dense potential core in supercritical injection: a thermal break-up mechanism. *Phys. Fluids* **28** (3), 035103.

BLUMEN, W. 1970 Shear layer instability of an inviscid compressible fluid. *J. Fluid Mech.* **40** (4), 769–781.

CHUNG, T.H., LEE, L.L. & STARLING, K.E. 1984 Applications of kinetic gas theories and multiparameter correlation for prediction of dilute gas viscosity and thermal conductivity. *Ind. Engng Chem. Fundam.* **23** (1), 8–13.

GROSS, J. & SADOWSKI, G. 2001 Perturbed-chain SAFT: an equation of state based on a perturbation theory for chain molecules. *Ind. Engng Chem. Res.* **40** (4), 1244–1260.

KEE, R.J., COLTRIN, M.E. & GLARBORG, P. 2005 *Chemically Reacting Flow: Theory and Practice*. John Wiley & Sons.

KOUKOUVINIS, P., VIDAL-RONCERO, A., RODRIGUEZ, C., GAVAISES, M. & PICKETT, L. 2020 High pressure/high temperature multiphase simulations of dodecane injection to nitrogen: Application on ECN spray-A. *Fuel* **275**, 117871.

LUX, J. & HAIDN, O. 2009 Flame stabilization in high-pressure liquid oxygen/methane rocket engine combustion. *J. Propul. Power* **25** (1), 15–23.

LY, N., RUSAK, Z. & WANG, S. 2018 Swirling flow states of compressible single-phase supercritical fluids in a rotating finite-length straight circular pipe. *J. Fluid Mech.* **849**, 576–614.

MACLAURIN, D., DUVENAUD, D. & ADAMS, R.P. 2015 Autograd: effortless gradients in numpy. In *ICML 2015 AutoML Workshop*, vol. 238, pp. 1–5.

MAYER, W., TELAAR, J., BRANAM, R., SCHNEIDER, G. & HUSSONG, J. 2003 Raman measurements of cryogenic injection at supercritical pressure. *Heat Mass Transfer* **39** (8), 709–719.

MICHALKE, A. 1972 The instability of free shear layers. *Prog. Aerosp. Sci.* **12**, 213–216.

OSCHWALD, M., SMITH, J.J., BRANAM, R., HUSSONG, J., SCHIK, A., CHEHROUDI, B. & TALLEY, D. 2006 Injection of fluids into supercritical environments. *Combust. Sci. Technol.* **178** (1–3), 49–100.

REN, J., FU, S. & PECNIK, R. 2019*a* Linear instability of Poiseuille flows with highly non-ideal fluids. *J. Fluid Mech.* **859**, 89–125.

REN, J., MARXEN, O. & PECNIK, R. 2019*b* Boundary-layer stability of supercritical fluids in the vicinity of the widom line. *J. Fluid Mech.* **871**, 831–864.

ROY, A. & SEGAL, C. 2010 Experimental study of fluid jet mixing at supercritical conditions. *J. Propul. Power* **26** (6), 1205–1211.

SCHMID, P.J. & HENNINGSON, D.S. 2001 *Stability and Transition in Shear Flows*. Springer.

SIMEONI, G.G., BRYK, T., GORELLI, F.A., KRISCH, M., RUOCCO, G., SANTORO, M. & SCOPIGNO, T. 2010 The Widom line as the crossover between liquid-like and gas-like behaviour in supercritical fluids. *Nat. Phys.* **6** (7), 503–507.

TAKAHASHI, S. 1975 Preparation of a generalized chart for the diffusion coefficients of gases at high pressures. *J. Chem. Engng Japan* **7** (6), 417–420.

ZONG, N., MENG, H., HSIEH, S.-Y. & YANG, V. 2004 A numerical study of cryogenic fluid injection and mixing under supercritical conditions. *Phys. Fluids* **16** (12), 4248–4261.